ACS Photonics

pubs.acs.org/journal/apchd5

Letter

Label-Free Optical Microscope Based on a Phase-Modulated Femtosecond Pump−Probe Approach with Subdiffraction Resolution

Amir Fathi, Chao-Yu Chung, Yuan-Pern Lee, and Eric Wei-Guang Diau*

Cite This: *ACS Photonics* 2020, 7, 607−613

Read Online

ACCESS | Metrics & More | Article Recommendations | Supporting Information

ABSTRACT: A far-field optical microscope (OM) is a powerful noninvasive, nondestructive tool to study sub-micrometer structures and organisms, which has been used for decades to study the interactions between light and matter in the spatial domain. We report here a sophisticated label-free OM method with superspatial resolution to visualize ZnO nanoparticles. Of three femtosecond pulses, two served as pumps at 1000 nm and the other one served as a probe at 774 nm. The two pumps (one of Gaussian shape and the other of toroidal shape) were generated with a phase difference of 180°. When the conventional pump−probe approach was used in the absence of a second toroidal pump, a ZnO nanoparticle was observed to show a particle size of 445 nm because of the limit of diffraction. In contrast, when the second toroidal pump was applied out of phase, the obtained OM image showed a ZnO nanoparticle down to 96 nm. We demonstrated for the first time that the reported phase-modulated pump−probe approach has an ability for spatial resolution beyond its optical diffraction limit and a potential for label-free imaging applications in nanomaterials and life sciences.

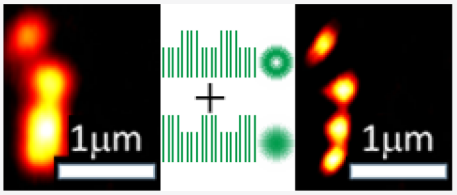

KEYWORDS: *laser scanning microscope, optical microscopy, pump−probe imaging, super-resolution, ultrafast microscopy*

Downloaded via NATL CHIAO TUNG UNIV on March 18, 2020 at 10:06:26 (UTC).
See https://pubs.acs.org/sharingguidelines for options on how to legitimately share published articles.

The far-field optical microscope (OM) has been extensively utilized as a noninvasive tool to study and to visualize biological or nanoparticle systems in condensed matter,[1] but the spatial resolution is limited by the optical principle reported by Ernst Abbe.[2] For a few decades, even with the advance of a confocal system, the spatial resolution of a optical microscope was still limited to ∼250 and ∼500 nm for lateral and axial positions, respectively.[3] To overcome this fundamental barrier, many scientists have engaged to find a solution by mathematical modeling,[4] an algorithmic approach,[5] adding another laser beam to deplete the excited state,[6] or employing a physical phenomenon to eliminate the edge region and to maintain the central region[7] to increase the spatial resolution. This approach has been done with not only a fluorescent microscope but also four-wave mixing (FWM),[8] coherent anti-Stoke Raman scattering (CARS),[8] and transient absorption (TA)[9] microscopic techniques.[10,11]

Ash and Nicolls[12] first achieved subdiffraction (subwavelength) spatial resolution in 1972 on scanning the near-field evanescent wave from a metal grating. In this configuration, the resolution depends on the aperture and the evanescent wave, not the wavelength of the illuminating radiation. Although in their experiment illumination microwaves were utilized, many other scanning optical-microscope techniques followed.[13−15] Inspired by a typical medical stethoscope, Pohl et al.[13] illustrated an optical stethoscope technique that achieved a resolving power of $\lambda/20$. The same group subsequently introduced a near-field optical-scanning microscope (NFOS)[14] with which a resolution of 20 nm was reported. Betzig et al.[15] introduced a scanning near-field optical microscope (SNOM) that was inspired by the work of Lewis et al.[16] Despite their high-resolution capabilities,[17] research progress was slow because of difficulties in engineering tips for these near-field OM techniques. SNOM coupled with an atomic-force microscope (AFM) becomes a powerful tool to study material images on a nanometer scale using a near-field evanescent wave, but it is inapplicable to all situations and samples because of the difficulty of tip engineering and a lack of images in the axial direction.

Returning to a far-field microscope, an early effort was expended by Hell and Stelzer[18] through superimposition of two beams on the focal plane as an excitation source to increase the axial optical resolution; this method improved the optical sectioning. They subsequently proposed a stimulated emission depletion microscope (STED)[6,19,20] technique to achieve a resolution of ∼35 nm on shrinking the size of the fluorescing spot in the excited state via a stimulated emission with a toroidal beam. Another technique, ground-state

Received: December 24, 2019
Published: March 5, 2020

© 2020 American Chemical Society

https://dx.doi.org/10.1021/acsphotonics.9b01821
ACS Photonics 2020, 7, 607−613

Table 1. Summary of Varied Super-resolution Optical Microscope Methods Reviewed in This Article

methods	resolution/nm	remarks	references
NFOS,[a] SNOM[b]	∼20	acquisition is slow; tip is fragile and difficult to make; 3D sectioning is impracticable (near-field OM)	14, 15
STED,[c] GSD,[d] RESOLFT[e]	<35	a third beam is necessary to saturate, to deplete, or to channel the transition; marker staining or labeling is required	6, 19−22
SIM,[f] SSIM[g]	∼100, ∼50	the resolution enhancement is small; computation and postprocessing are required; processing might cause artifacts	24, 25
PALM,[h] STORM[i]	∼20	marker staining or labeling is required; acquisition is slow; data storage is necessary; postprocessing is required	4, 25, 26
CARS[j] (phase manipulation)	∼130	manipulating the phase distribution at a focal plane might cause artifacts	8
saturable scattering	∼70	intense femtosecond pulses are required to saturate electronic transitions that might cause photochemical damage of a target sample	36, 37
TAM[k] (saturating the transition)	∼225	a target sample is selective on an optical absorption property; saturating the transition is required, which might cause photochemical damage of the sample	38
TAM[k] (differential detection)	∼270	the target sample is selective and prone to photochemical damage; spatial resolution is poor	9
PM-FPPM[l]	<100	broad selectivity of label-free samples is capable in a pump−probe scheme with phase modulation of the two pump beams	this work

[a]Near-field optical scanning. [b]Scanning near-field optical microscopy. [c]Stimulated emission depletion. [d]Ground-state depletion. [e]Reversible saturable optical fluorescence transitions. [f]Structured illumination microscopy. [g]Saturated structured illumination microscopy. [h]Photoactivable localization microscopy. [i]Stochastic reconstruction microscopy. [j]Coherent anti-Stokes Raman scattering. [k]Transient absorption microscopy. [l]Phase-modulated femtosecond pump−probe microscopy.

depletion microscopy (GSD),[21] surpasses the diffraction limit, with CW lasers less intense than for STED on shelving the fluorophores at the peripheral region in the nonfluorescing states (triplet states), of which the lifetime (μs to ms) is greater than for their fluorescing state (∼ns); resolution to 50 nm was demonstrated. Using the same principle, another group imaged color centers of diamonds as small as 7.6 nm through GSD.[22] Under a more general acronym, RESOLFT, denoting reversible saturable optical fluorescence transitions,[23] a photoswitchable protein can serve as a marker that has an off-state in the peripheral region; only the central part contributes to the image of fluorescence. Spatial resolution between 50 and 100 nm was achievable with less laser intensity to terminate the fluorescence of proteins.[15]

A structured illumination microscope (SIM)[24,25] is another approach that doubled the spatial resolution (to ∼100 nm) laterally. In this technique, a sample is illuminated with patterns in a series of formed sinusoidal strips that can yield a super-resolved image after postprocessing the images in the acquired set. A grating or a spatial light modulator (SLM) was used to generate the required structured illumination fields; the increased component of spatial frequency can then be extracted from the emission to achieve a subdiffraction limit. With this approach and an improved alignment, the authors achieved a resolution of less than 50 nm on saturating the fluorescence transitions using an intense beam for excitation.[25] In 2006, Betzig et al.[26] introduced an OM technique named wide-field super-resolution fluorescence photoactivable localization microscopy (PALM); Rust et al.[4] concurrently developed a similar approach to attain subdiffraction-limited resolution with an OM technique called stochastic reconstruction microscopy (STORM). The basic principle of PALM and STORM lies in the use of photoswitchable fluorescent molecules that are iteratively switched on and off. The fluorescent molecules are initially in the off-state (dark state) and can then be switched to an on-state (bright state) with weak illumination; under this condition and a stochastic nature of the distribution of the emitting points at each taken shot, the position of molecules is pin-pointed with a mathematical model. After sufficient shots, the overlay of all images results in a super-resolution image beyond what is achievable with a traditional confocal microscope. The key point is that the excitation should be weak enough that two (or more) emitting points are separable to an extent greater than the diffraction limit at each shot; data can then be fitted precisely.

These far-field OM techniques were developed using the idea of a fluorescent signal that is inapplicable to many systems such as thin-film samples or living cells that lack a fluorescent marker. In general, even though a fluorescence-marker system can achieve increased spatial resolution, the approaches such as SIM, PALM, and STORM require postprocessing that can cause artifacts in the images. Moreover, these methods require protracted data acquisition; the data stream is large and requires gigabytes of rapid storage for each measurement. In the approaches of RESOLFT, STED, GSD, and so forth, an intense laser beam for photoactive switching causes stimulated emission or ground-state depletion. The success of these techniques has motivated other researchers to adopt other approaches to break the diffraction limit with varied OM techniques that require neither staining nor the use of a second intense beam, e.g., CARS,[27,28] stimulated Raman scattering (SRS),[29] second-harmonic generation (SHG)[30] and third-harmonic generation (THG),[31] TA microscopy,[32] and so forth.

To improve the resolution capability for CARS and SRS microscopic techniques, Beeker et al.,[33] in a theoretical study, proposed using a third toroidal beam to suppress the vibrational coherence so that only the central part of a focal field emits a CARS signal. According to their calculation, an upper limit for the improved resolution was estimated to be $\sim\lambda/(2 \times \mathrm{NA})$, in which the probe beam has wavelength λ and NA represents the numerical aperture. The same group, in another theoretical approach, suggested depleting the ground-state population periodically through Rabi oscillations with a controlled third beam.[34] Based on their calculations, a spatial resolution of 65 nm is practicable. The calculation is valid for a two-level system in a real case, but various transitions can cause decoherence; Rabi oscillation hence does not occur to suppress the CARS signal at the peripheral region.

Raghunathan and Potma[35] estimated that, on appropriately shaping the Stokes phase to have a phase distribution of

https://dx.doi.org/10.1021/acsphotonics.9b01821
ACS Photonics 2020, 7, 607−613

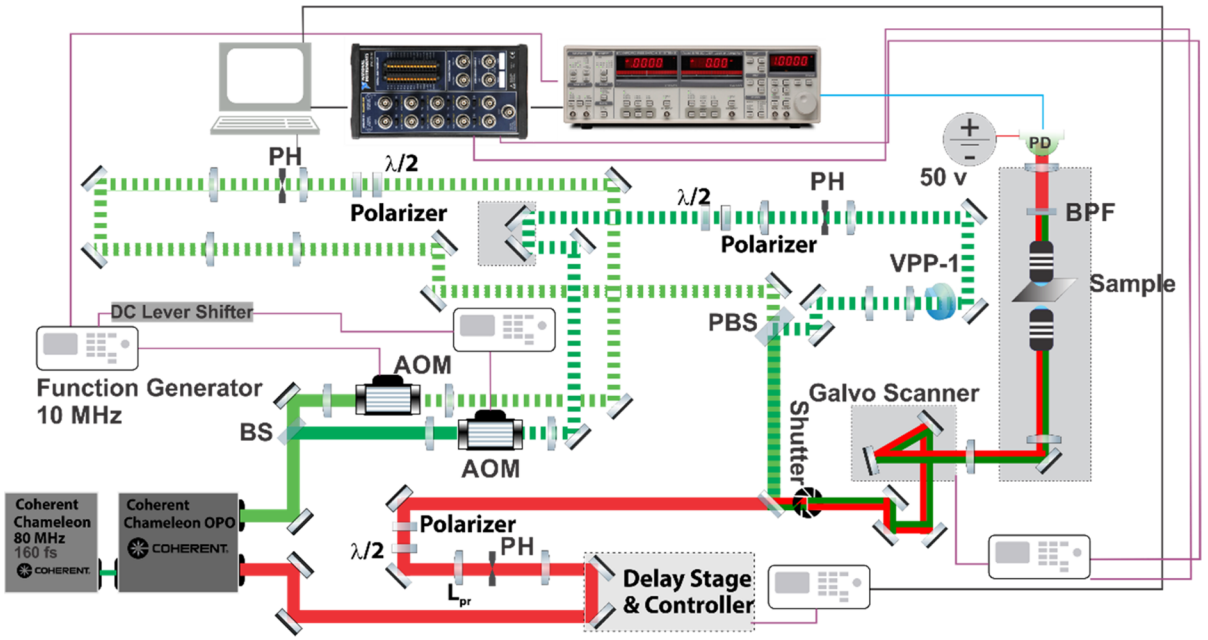

Figure 1. Experimental setup for optical imaging with a phase-modulated femtosecond pump−probe microscope (PM-FPPM). The pulse train of a laser source (80 MHz) that is modulated at 10 MHz for the pump and unmodulated for the probe, with the spatial profile at the focal plane. BS: 50:50 beam splitter; AOM: acousto-optical modulator; BPF: bandpass filter (600−900 nm); PBS: polarization beam splitter; PD: photodiode; PH: pinhole; T: telescope; VPP-1: vortex phase plate; L_{pr}: the probe lens to tune the axial offset.

toroidal type, which contains a π-phase in the central region and zero phase in the annular region, the optical resolution of a CARS microscope can be improved by half. In 2012, Kim et al.[8] experimentally realized Raghunathan's idea and demonstrated an optical resolution of 130 nm for an FWM microscope, but the practical resolution limit for complicated features might hinder further applications through artifacts caused by a large side-lobe of the image. On saturating the scattering of gold nanoparticles, Chu et al.[36,37] achieved, by extracting higher harmonics—second or third harmonics—of modulation of the flattened signals, a $\lambda/8$ point-spread function (PSF) of well-separated particles. Although the applications require labeling the sample with a gold nanoparticle, this method is less cytotoxic in cell-biology imaging. The use of intense short laser pulses is also an issue that might cause artifacts or degradation during the imaging.

Digressing from methods based on nonlinear scattering, Wang et al.[38] used an unmodulated toroidal laser beam to saturate the electronic transitions in the periphery so that the probe beam was modulated only in the center. With this high-speed imaging technique, they showed subdiffraction images of graphite nanoplatelets enhanced to order 0.6 relative to a conventional TA microscope. The sample imaged in this setup must be a saturable absorber, so that the transition became saturated without photochemical damage. Liu et al.[9] introduced a label-free solution to increase resolution in a differential way; to avoid saturating the transitions, they used a toroidal laser beam of different wavelength with a negative TA signal and collected only the positive TA signal from the center. They hence measured CdSe nanorods with a spatial resolution of ∼270 nm, which is much greater than the regular OM measurement of spatial resolution ∼850 nm.

The techniques summarized in Table 1 focus mainly on either shaping a phase distribution of laser beams via saturating the electronic or vibrational transitions or suppressing monitoring signals through generation of separate channels to achieve super-resolution of an OM image. In techniques in which emission from targeted samples is acquired, one way is to suppress the emission of the emissive species at the periphery. For this purpose, a toroidal shape is employed to depopulate the excited state through various mechanisms such as stimulated emission. In these techniques, the smallest feature that can be resolved is determined not by the diffraction limit but by the intensity of a third beam. These techniques are consequently applicable only for emissive samples or for samples with marking and labeling species. Furthermore, the intense third beam might cause photochemical damage to a target sample if not conducted well. In other approaches of fluorescent microscopes, in which tunable markers were used under the pump beam with minute excitation intensity, besides the labeling requirement, the protracted acquisition, large data storage, and extensive data processing postimaging are disadvantages. In a nonlinear OM approach, for channeling the source of the signal to increase the resolution, a large pump intensity is required for the target sample with a small absorption cross section, which can cause sample deterioration during the processing. In addition, if beam-shaping is necessary, artifacts can have a strong influence on the features of the image. If a particular optical property is targeted such as in a TA microscope, photobleaching or excited-state absorption should be considered for proper selection of a sample. Because photodegradation is an important issue, we present here a new route to feature superspatial resolution below the optical diffraction limit in a label-free manner with an approach involving a phase-modulated femtosecond pump−probe microscope (PM-FPPM). The idea is to create a summation of two signals in which the in-phase signal can be generated from the central region and out-of-phase signal generated from the toroidal region of the image; we can then map the object with increased spatial resolution by masking the image and clipping the negative signal. Various phenomena can be targeted as they

https://dx.doi.org/10.1021/acsphotonics.9b01821
ACS Photonics 2020, 7, 607−613

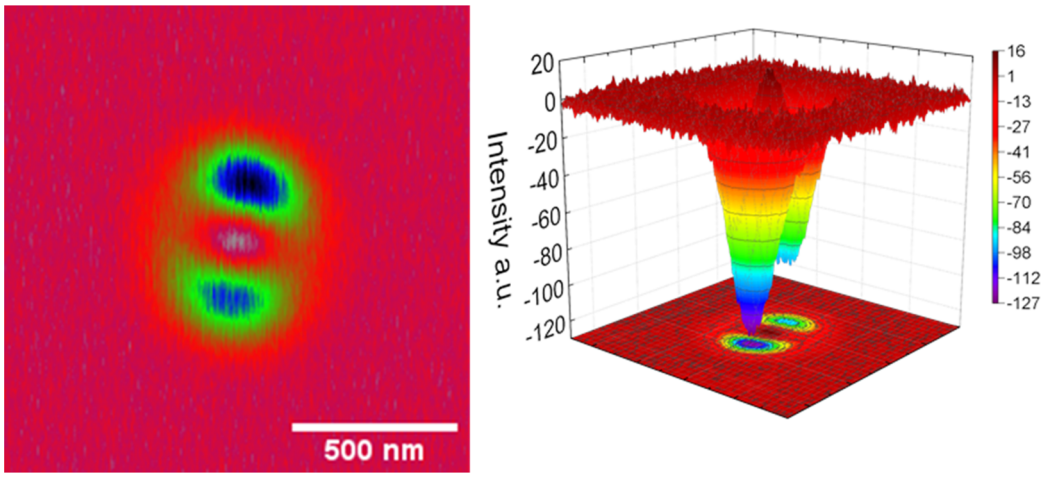

Figure 2. Top view (left) of the engineered PSF (ePSF) and its surface plot (right) when summing the two probe signals (modulated with two pump beams) at the focal plane.

can be implemented within a pump−probe scheme. In this scenario, because there is no need for channeling the transition or saturation, an intense beam at the peripheral region is not required. A broad selection of samples can be studied because no staining or labeling is required.

EXPERIMENTS

The experiment for the subdiffraction PM-FPPM technique is shown in Figure 1. The pump beam at 1000 nm was generated with an optical parametric oscillator (Chameleon OPO, Coherent) pumped with a Ti-sapphire laser (Chameleon, Coherent) at 774 nm. The selection of pump/probe wavelengths is arbitrary, and we selected 1000 nm/774 nm in our system for the purpose of alignment so that the C−H stretching band of an oil sample can be monitored via the effect of stimulated Raman scattering. The selection of 1000 nm for the pump beam is due to the use of a vortex phase plate (VPP-1, RPC photonics) to generate a toroidal beam detailed below. After separation of the pump beam into two beams with a 50:50 beam splitter (BS), the two pump beams passed separately through two acoustic-optical modulators (AOM, Gooch & Housego) modulated at 10 MHz with two individual function generators (RS345, Stanford Research). The first-order output from two intensity-modulated pump beams, with a phase difference of 180°, was collected. One pump beam passed through the VPP-1 plate to generate a helical phase of retardation from 0 to 2π, leading to a toroidal beam shape. The two pump beams at 1000 nm were then recombined with a 50:50 beam splitter and further collinearly overlapped by means of a dichroic mirror with the probe beam at 774 nm. The delay between pump and probe beams was controlled with a delay stage (Suruga Seiki KS102-100). To avoid interference between the two pump beams, their polarizations were set perpendicular to one another. These three collinear beams were then directed to a galvo scanner (6210H, Cambridge Technology) and focused onto the sample with an objective (60×, NA 1.2, Olympus). The transmitted probe beam was collected with a condenser (40× objective, NA 0.9), filtered with two short-pass filters (FES0950, Thorlabs), and detected with a photodiode (FDS1010, Thorlabs) biased at 50 V. The output from the photodiode was further filtered with an electronic band-pass filter (BBP-10.7+, Mini-circuit) and then fed into a lock-in amplifier (SR844, Stanford Research Systems) to extract the pump−probe signal at 10 MHz. A data acquisition card (PCIe6251, National Instruments) was used not only to control the scanning angles of the galvo scanner but also to record synchronously the voltage outputs from the amplifier. The pixel dwell period is ∼40 μs, which was limited by our data acquisition board when the lock-in amplifier filter was set to the "no time-constant" mode. The image acquisition program was written with software (Labview, National Instruments). We evaluated the dimensions of the field of view with a microscope calibration slide. To obtain a toroidal mode at the focal plane with a uniform distribution, it is important to clean the wavefront with a spatial filter and ensure that the beam is linearly polarized before the wave plate; before focusing the beam, the polarization should be set in a circular mode for the best result. A comparison between the circularly and linearly polarized lights based on a simulation is presented in Figure S1, Supporting Information (SI). In this configuration, the instrument response function (IRF) was estimated to be ∼500 fs by measuring the cross-correlation response of the C−H stretching band of the oil sample. The laser fluence used throughout the experiments was ∼1 mJ cm^{-2} for pump and ∼3 mJ cm^{-2} for probe.

RESULTS AND DISCUSSION

The same configuration is useful for many pump−probe measurements, such as transient absorption or two-photon absorption, on selecting appropriate pump and probe wavelengths. As this scheme has a generic nature, in principle time-resolved data with increased spatial resolution is achievable. To achieve subdiffraction resolution, we modulated the probe with two pump beams, both of which had a phase difference of 180° resulting in the summation of two modulated probes at the focal plane. In this detection scheme, the positive signal was generated with the probe that was modulated with the Gaussian mode pump. The negative signal originated from the probe that was modulated with the toroidal-shaped pump, because of how a lock-in amplifier detected the out-of-phase signal. The signal detected here was the thermal lensing effect from a sample made of drop-cast zinc oxide (ZnO) nanoparticles (Sigma-Aldrich 721077, average particle size ∼40 nm) on a microscope coverslip. The thermal lensing effect is the modulation in the intensity of the probe beam induced by the pump beam via changing the refractive index of the

https://dx.doi.org/10.1021/acsphotonics.9b01821
ACS Photonics 2020, 7, 607−613

nanoparticle temporarily. To obtain the maximum thermal lensing signal, the probe beam requires an axial offset with respect to the pump beam at the focal plane. To control this axial offset, the probe lens (L_{pr}) was mounted on a translational stage and used for fine-tuning of the signal level.[39,40] The overall signal was a summation of in-phase and out-of-phase signals, but we consider only the positive (in-phase) signal. The positive Gaussian signal minus the toroidal signal is what we observed in the field of view. On tuning the powers of toroidal and Gaussian beams, we can attain spatial resolution beyond the diffraction limit. As shown in Figure 2, we can easily engineer two pump beams to obtain an engineered PSF (ePSF) at the focal plane to achieve an increased spatial resolution.

As a proof of concept, Figure 3a shows a direct pump−probe nonresonance scattering image of a single ZnO nanoparticle

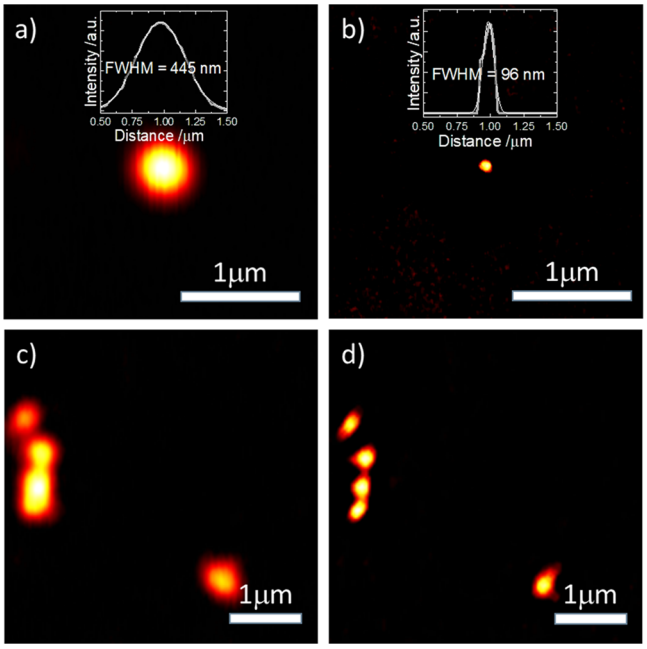

Figure 3. Comparison of images (a) without and (b) with the toroidal profile pump. For (a), the resolution calculated on fitting the line profile to a Gaussian function results in an fwhm of 445 ± 1 nm; for (b), the fwhm is 96 ± 1 nm. (c and d) Images without and with the toroidal pump beams, respectively, for multiple nanoparticles (on the left side) when they are located near each other.

without introducing the toroidal pump, for which the fwhm was estimated to be 445 ± 1 nm on fitting the line profile with a Gaussian function. After the second pump beam was introduced, Figure 3b shows the fwhm significantly decreased to 96 ± 1 nm. In this detection scheme it was crucial to determine the phase accurately to avoid distortion of the toroidal signal at the focal plane. Because this technique does not reflect the true size of a particle, as sizes smaller than the original ones can be achieved on engineering the PSF accordingly, to avoid artifacts, the intensity ratio of the two pumps must be calibrated before the measurements (Figure S2, SI). Here, we showed that a ZnO nanoparticle can be visualized beyond the diffraction limit without postprocessing and with an acquisition speed of 0.8 s per frame (for size 256 × 256 pixels). We further demonstrate the resolution enhancement on showing the images of three closely located ZnO nanoparticles with and without introduction of the toroidal pump. Three aligned particles on the left side of Figure 3c are not spatially resolved in a conventional setup without the toroidal pump. In contrast, Figure 3d shows that, on introducing the second pump in the toroidal mode, the three nanoparticles are fully resolved. We emphasize the significance of our PM-FPPM approach to improve the spatial resolution beyond the optical diffraction limit free of labeling with an emissive dye. Line profiles of the three particles shown in Figures 3c and d are shown in Figure S3a and b, SI, respectively, for clear comparison between the two cases.

This method is applicable to any other pump−probe microscope technique, such as TA, two-photon absorption, SRS, FWM, and so on, to enhance the spatial resolution beyond the diffraction limit because only the PSF is modified within the scheme of detection. Because there is no other laser beam to saturate, to depopulate, to inactivate, or to channel the probed phenomenon, the disadvantages of artifact issues, such as tedious measurement, computationally intensive processing, and photochemical damage, are absent. Additionally, in the case of a TA microscope, as the kinetics are left intact without forced relaxation to the ground state (or intermediate state), the time-resolved data of the image can be recorded.

As demonstrated here only for ZnO nanoparticles, this technique is applicable to other nanoparticle or quantum-dot samples. In the following we discuss some prospective applications in which nanoparticles serve for various purposes. When they are present in a system, their signal generated can also be used to visualize the system. Nanoparticles and nanorods, such as gold, have become useful markers in many branches of cell biology. In high-resolution label-free imaging techniques, they can hence become a powerful tool to study the relaxation dynamics inside a living cell. Gold nanoparticles were used for cancer-cell apoptosis,[41] but, to monitor the effectiveness, the tests were undertaken on staining the treated cell with fluorescent proteins. Inorganic metal-based nanoparticles in the form of nanoshells or nanocages can be functionalized for gene and drug delivery,[42] hyperthermia-based therapeutics,[43] and others,[44] but their functions were monitored through other imaging techniques. Gold nanoparticles, for their surface-enhanced Raman-scattering (SERS) character, served extensively as a probe in stem-cell research,[45−47] but, to ensure the delivery to the targeted cell, a transmission electron microscope (TEM) was used with a stimulated-Raman scattering microscope in a confocal laser scanning system. As reported elsewhere,[48] to monitor uptake routes, hyperspectral SRS imaging was performed to demonstrate the multiple complications in studies of breast-cancer cells.[49] In these setups, near-IR laser sources were necessary, which limited the resolution to $\lambda/(0.6\times \mathrm{NA})$; the spatial resolution might be increased to ∼0.5 μm. Based on our results, as a prospective application, the subdiffraction PM-FPPM technique is suitable as a noninvasive approach with no necessity to stain cells to enhance the understanding of various drug−cell interactions with superior spatial and time resolutions.

CONCLUSION

We present here a brief comparison of various super-resolution optical microscopic techniques including their advantages and limitations with their current and prospective applications. The usage of a toroidal beam, based on its wavelength and intensity, was designed to meddle with the diffraction-limited point-spread function, to eliminate the source of a signal in its

https://dx.doi.org/10.1021/acsphotonics.9b01821
ACS Photonics 2020, 7, 607−613

peripheral region. Here we introduced a subdiffraction far-field OM technique based on a phase-modulated femtosecond pump−probe scheme taking advantage of the summation nature of in-phase and out-of-phase signals from a lock-in amplifier. The turn-off state at the toroidal region does not occur, as the enhancement results from the heterodyne detection of two modulated signals at a phase difference of 180°. On modulating the toroidally shaped pump beam at 180° with respect to the Gaussian pump beam, we detected a single ZnO nanoparticle with subdiffraction spatial resolution (<100 nm) and distinguished closely located multiple nanoparticles beyond the optical diffraction limit. This approach is applicable to many other OM techniques for tracking and visualization objects in a system of interest. The spatial resolution depends on the modulation depth ratio between the two beams at the focal plane caused by the two pumps. After calibration, fine structures can be resolved below the diffraction limit in a rapid frame scan. This label-free OM technique is intrinsically due to the effect of thermal lensing in a way similar to a nonresonance scattering phenomenon; it might be modified according to a resonance-stimulated Raman-scattering approach with a potential to apply in many other bioimaging and nanomaterial systems with subdiffraction spatial and femtosecond time resolutions.

■ ASSOCIATED CONTENT

Supporting Information

The Supporting Information is available free of charge at https://pubs.acs.org/doi/10.1021/acsphotonics.9b01821.

Additional figures showing laser intensity distribution at the focal plane, calibration of the power ratios, and line profiles of three nanoparticles (PDF)

■ AUTHOR INFORMATION

Corresponding Author

Eric Wei-Guang Diau − *Department of Applied Chemistry and Institute of Molecular Science and Center for Emergent Functional Matter Science, National Chiao Tung University, Hsinchu 30010, Taiwan;* orcid.org/0000-0001-6113-5679; Email: diau@mail.nctu.edu.tw

Authors

Amir Fathi − *Department of Applied Chemistry and Institute of Molecular Science, National Chiao Tung University, Hsinchu 30010, Taiwan;* orcid.org/0000-0002-2528-8405

Chao-Yu Chung − *Department of Applied Chemistry and Institute of Molecular Science, National Chiao Tung University, Hsinchu 30010, Taiwan*

Yuan-Pern Lee − *Department of Applied Chemistry and Institute of Molecular Science and Center for Emergent Functional Matter Science, National Chiao Tung University, Hsinchu 30010, Taiwan;* orcid.org/0000-0001-6418-7378

Complete contact information is available at: https://pubs.acs.org/10.1021/acsphotonics.9b01821

Notes

The authors declare no competing financial interest.

■ ACKNOWLEDGMENTS

We thank Dr. Yin-Yu Lee from National Synchrotron Radiation Research Center (NSRRC) for his support in setting up the microscope system. Taiwan Ministry of Science and Technology (MOST) provided financial support of this research (MOST 105-2119-M-009-011-MY3, MOST 107-2119-384 M-009-001, and MOST 108-2119-M-009-004). This work was financially supported also by the Center for Emergent Functional Matter Science of National Chiao Tung University from The Featured Area Research Center Program within the framework of the Higher Education SPROUT Project by Taiwan Ministry of Education (MOE).

■ REFERENCES

(1) Renz, M. Fluorescence Microscopy-A Historical and Technical Perspective. *Cytometry, Part A* **2013**, *83*, 767−779.

(2) Abbe, E. Beiträge Zur Theorie Des Mikroskops Und Der Mikroskopischen Wahrnehmung. *Arch. für Mikroskopische Anat.* **1873**, *9*, 413−418.

(3) *Handbook of Biological Confocal Microscopy*; Pawley, J. B., Ed.; Springer US: Boston, MA, 2006.

(4) Rust, M. J.; Bates, M.; Zhuang, X. Sub-Diffraction-Limit Imaging by Stochastic Optical Reconstruction Microscopy (STORM). *Nat. Methods* **2006**, *3*, 793−796.

(5) Richardson, W. H. Bayesian-Based Iterative Method of Image Restoration. *J. Opt. Soc. Am.* **1972**, *62*, 55.

(6) Hell, S. W.; Wichmann, J. Breaking the Diffraction Resolution Limit by Stimulated Emission: Stimulated-Emission-Depletion Fluorescence Microscopy. *Opt. Lett.* **1994**, *19*, 780.

(7) Klar, T. A.; Jakobs, S.; Dyba, M.; Egner, A.; Hell, S. W. Fluorescence Microscopy with Diffraction Resolution Barrier Broken by Stimulated Emission. *Proc. Natl. Acad. Sci. U. S. A.* **2000**, *97*, 8206−8210.

(8) Kim, H.; Bryant, G. W.; Stranick, S. J. Superresolution Four-Wave Mixing Microscopy. *Opt. Express* **2012**, *20*, 6042.

(9) Liu, N.; Kumbham, M.; Pita, I.; Guo, Y.; Bianchini, P.; Diaspro, A.; Tofail, S. A. M.; Peremans, A.; Silien, C. Far-Field Subdiffraction Imaging of Semiconductors Using Nonlinear Transient Absorption Differential Microscopy. *ACS Photonics* **2016**, *3*, 478−485.

(10) Huang, B.; Babcock, H.; Zhuang, X. Breaking the Diffraction Barrier: Super-Resolution Imaging of Cells. *Cell* **2010**, *143*, 1047−1058.

(11) Huang, B.; Bates, M.; Zhuang, X. Super-Resolution Fluorescence Microscopy. *Annu. Rev. Biochem.* **2009**, *78*, 993−1016.

(12) Ash, E. A.; Nicholls, G. Super-Resolution Aperture Scanning Microscope. *Nature* **1972**, *237*, 510−512.

(13) Pohl, D. W.; Denk, W.; Lanz, M. Optical Stethoscopy: Image Recording with Resolution $\lambda/20$. *Appl. Phys. Lett.* **1984**, *44*, 651−653.

(14) Dürig, U.; Pohl, D. W.; Rohner, F. Near-field Optical-scanning Microscopy. *J. Appl. Phys.* **1986**, *59*, 3318−3327.

(15) Betzig, E.; Lewis, A.; Harootunian, A.; Isaacson, M.; Kratschmer, E. Near Field Scanning Optical Microscopy (NSOM). *Biophys. J.* **1986**, *49*, 269−279.

(16) Lewis, A.; Isaacson, M.; Harootunian, A.; Muray, A. Development of a 500 Å Spatial Resolution Light Microscope. *Ultramicroscopy* **1984**, *13*, 227−231.

(17) Betzig, E.; Trautman, J. K.; Harris, T. D.; Weiner, J. S.; Kostelak, R. L. Breaking the Diffraction Barrier: Optical Microscopy on a Nanometric Scale. *Science* **1991**, *251*, 1468−1470.

(18) Hell, S.; Stelzer, E. H. K. Fundamental Improvement of Resolution with a 4Pi-Confocal Fluorescence Microscope Using Two-Photon Excitation. *Opt. Commun.* **1992**, *93*, 277−282.

(19) Hell, S. W. Far-Field Optical Nanoscopy. *Science* **2007**, *316*, 1153−1158.

(20) Hell, S. W.; Kroug, M. Ground-State-Depletion Fluorscence Microscopy: A Concept for Breaking the Diffraction Resolution Limit. *Appl. Phys. B: Lasers Opt.* **1995**, *60*, 495−497.

(21) Bretschneider, S.; Eggeling, C.; Hell, S. W. Breaking the Diffraction Barrier in Fluorescence Microscopy by Optical Shelving. *Phys. Rev. Lett.* **2007**, *98*, 218103.

(22) Rittweger, E.; Wildanger, D.; Hell, S. W. Far-Field Fluorescence Nanoscopy of Diamond Color Centers by Ground State Depletion. *EPL (Europhysics Lett.* **2009**, *86*, 14001.
(23) Hofmann, M.; Eggeling, C.; Jakobs, S.; Hell, S. W. Breaking the Diffraction Barrier in Fluorescence Microscopy at Low Light Intensities by Using Reversibly Photoswitchable Proteins. *Proc. Natl. Acad. Sci. U. S. A.* **2005**, *102*, 17565−17569.
(24) Gustafsson, M. G. L. Surpassing the Lateral Resolution Limit by a Factor of Two Using Structured Illumination Microscopy. *J. Microsc.* **2000**, *198*, 82−87.
(25) Heintzmann, R.; Cremer, C. G. Laterally Modulated Excitation Microscopy: Improvement of Resolution by Using a Diffraction Grating. In *Optical Biopsies and Microscopic Techniques III*; Bigio, I. J., Schneckenburger, H., Slavik, J., Svanberg, K., Viallet, P. M., Eds.; SPIE: Bellingham, WA, 1999; pp 185−196.
(26) Betzig, E.; Patterson, G. H.; Sougrat, R.; Lindwasser, O. W.; Olenych, S.; Bonifacino, J. S.; Davidson, M. W.; Lippincott-Schwartz, J.; Hess, H. F. Imaging Intracellular Fluorescent Proteins at Nanometer Resolution. *Science* **2006**, *313*, 1642−1645.
(27) Freudiger, C. W.; Min, W.; Saar, B. G.; Lu, S.; Holtom, G. R.; He, C.; Tsai, J. C.; Kang, J. X.; Xie, X. S. Label-Free Biomedical Imaging with High Sensitivity by Stimulated Raman Scattering Microscopy. *Science* **2008**, *322*, 1857−1861.
(28) Zumbusch, A.; Holtom, G. R.; Xie, X. S. Three-Dimensional Vibrational Imaging by Coherent Anti-Stokes Raman Scattering. *Phys. Rev. Lett.* **1999**, *82*, 4142−4145.
(29) Duncan, M. D.; Reintjes, J.; Manuccia, T. J. Scanning Coherent Anti-Stokes Raman Microscope. *Opt. Lett.* **2008**, *7*, 350.
(30) Chen, X.; Nadiarynkh, O.; Plotnikov, S.; Campagnola, P. J. Second Harmonic Generation Microscopy for Quantitative Analysis of Collagen Fibrillar Structure. *Nat. Protoc.* **2012**, *7*, 654−669.
(31) Débarre, D.; Supatto, W.; Pena, A.-M.; Fabre, A.; Tordjmann, T.; Combettes, L.; Schanne-Klein, M.-C.; Beaurepaire, E. Imaging Lipid Bodies in Cells and Tissues Using Third-Harmonic Generation Microscopy. *Nat. Methods* **2006**, *3*, 47−53.
(32) Grancini, G.; Polli, D.; Fazzi, D.; Cabanillas-Gonzalez, J.; Cerullo, G.; Lanzani, G. Transient Absorption Imaging of P3HT:PCBM Photovoltaic Blend: Evidence For Interfacial Charge Transfer State. *J. Phys. Chem. Lett.* **2011**, *2*, 1099−1105.
(33) Beeker, W. P.; Groß, P.; Lee, C. J.; Cleff, C.; Offerhaus, H. L.; Fallnich, C.; Herek, J. L.; Boller, K.-J. A Route to Sub-Diffraction-Limited CARS Microscopy. *Opt. Express* **2009**, *17*, 22632.
(34) Beeker, W. P.; Lee, C. J.; Boller, K.-J.; Groß, P.; Cleff, C.; Fallnich, C.; Offerhaus, H. L.; Herek, J. L. Spatially Dependent Rabi Oscillations: An Approach to Sub-Diffraction-Limited Coherent Anti-Stokes Raman-Scattering Microscopy. *Phys. Rev. A: At., Mol., Opt. Phys.* **2010**, *81*, 012507.
(35) Raghunathan, V.; Potma, E. O. Multiplicative and Subtractive Focal Volume Engineering in Coherent Raman Microscopy. *J. Opt. Soc. Am. A* **2010**, *27*, 2365−2374.
(36) Chu, S.-W.; Su, T.-Y.; Oketani, R.; Huang, Y.-T.; Wu, H.-Y.; Yonemaru, Y.; Yamanaka, M.; Lee, H.; Zhuo, G.-Y.; Lee, M.-Y.; et al. Measurement of a Saturated Emission of Optical Radiation from Gold Nanoparticles: Application to an Ultrahigh Resolution Microscope. *Phys. Rev. Lett.* **2014**, *112*, 017402.
(37) Lee, H.; Oketani, R.; Huang, Y.-T.; Li, K.-Y.; Yonemaru, Y.; Yamanaka, M.; Kawata, S.; Fujita, K.; Chu, S.-W. Point Spread Function Analysis with Saturable and Reverse Saturable Scattering. *Opt. Express* **2014**, *22*, 26016.
(38) Wang, P.; Slipchenko, M. N.; Mitchell, J.; Yang, C.; Potma, E. O.; Xu, X.; Cheng, J.-X. Far-Field Imaging of Non-Fluorescent Species with Sub-Diffraction Resolution. *Nat. Photonics* **2013**, *7*, 449−453.
(39) Selmke, M.; Braun, M.; Cichos, F. Photothermal Single-Particle Microscopy: Detection of a Nanolens. *ACS Nano* **2012**, *6*, 2741−2749.
(40) Devadas, M. S.; Devkota, T.; Johns, P.; Li, Z.; Lo, S. S.; Yu, K.; Huang, L.; Hartland, G. V. Imaging Nano-Objects by Linear and Nonlinear Optical Absorption Microscopies. *Nanotechnology* **2015**, *26*, 354001.
(41) Ramalingam, V.; Revathidevi, S.; Shanmuganayagam, T. S.; Muthulakshmi, L.; Rajaram, R. Gold Nanoparticle Induces Mitochondria-Mediated Apoptosis and Cell Cycle Arrest in Nonsmall Cell Lung Cancer Cells. *Gold Bull.* **2017**, *50*, 177−189.
(42) Ghosh, P.; Han, G.; De, M.; Kim, C. K. Gold Nanoparticles in Delivery Applications. *Adv. Drug Delivery Rev.* **2008**, *60*, 1307−1315.
(43) Peer, D.; Karp, J. M.; Hong, S.; Farokhzad, O. C.; Margalit, R.; Langer, R. Nanocarriers as an Emerging Platform for Cancer Therapy. *Nat. Nanotechnol.* **2007**, *2*, 751−760.
(44) Chithrani, D. B. Intracellular Uptake, Transport, and Processing of Gold Nanostructures. *Mol. Membr. Biol.* **2010**, *27*, 299−311.
(45) Sathuluri, R. R.; Yoshikawa, H.; Shimizu, E.; Saito, M.; Tamiya, E. Gold Nanoparticle-Based Surface-Enhanced Raman Scattering for Noninvasive Molecular Probing of Embryonic Stem Cell Differentiation. *PLoS One* **2011**, *6*, No. e22802.
(46) Kneipp, J.; Kneipp, H.; McLaughlin, M.; Brown, D.; Kneipp, K. In Vivo Molecular Probing of Cellular Compartments with Gold Nanoparticles and Nanoaggregates. *Nano Lett.* **2006**, *6*, 2225−2231.
(47) Kim, T.-H.; Lee, K.-B.; Choi, J.-W. 3D Graphene Oxide-Encapsulated Gold Nanoparticles to Detect Neural Stem Cell Differentiation. *Biomaterials* **2013**, *34*, 8660−8670.
(48) Huang, B.; Yan, S.; Xiao, L.; Ji, R.; Yang, L.; Miao, A.-J.; Wang, P. Label-Free Imaging of Nanoparticle Uptake Competition in Single Cells by Hyperspectral Stimulated Raman Scattering. *Small* **2018**, *14*, 1703246.
(49) Navas-Moreno, M.; Mehrpouyan, M.; Chernenko, T.; Candas, D.; Fan, M.; Li, J. J.; Yan, M.; Chan, J. W. Nanoparticles for Live Cell Microscopy: A Surface-Enhanced Raman Scattering Perspective. *Sci. Rep.* **2017**, *7*, 4471.

https://dx.doi.org/10.1021/acsphotonics.9b01821
ACS Photonics 2020, 7, 607−613